Research Article

Kondetharayil Soman, Kuppusamy Kanagaraj, Nangan Senthilkumar, Saravanan Rajendran*, Turki Kh. Faraj, Abdulwahed Fahad Alrefaei, Natesan Thirumalaivasan, Thanigaivel Sundaram*, Arpita Roy, Rajan Verma, Sabu Thomas, Sreeraj Gopi*, and Maximilian Lackner*

Nitrogen-doped carbon dots from Brahmi (*Bacopa monnieri*): Metal-free probe for efficient detection of metal pollutants and methylene blue dye degradation

https://doi.org/10.1515/gps-2024-0182
received August 16, 2024; accepted December 02, 2024

Abstract: Contaminants like heavy metals in water bodies pose serious risks to human health and ecosystems, often leading to acute and chronic disorders, including cancer and organ damage. Understanding water contamination is vital for sustainable development. A biosensor is a biocompatible, sustainable device that can detect heavy metal ions. To do this, we used a hydrothermal process to produce nitrogen-doped carbon dots (NCDs) from the plant Brahmi (*Bacopa monnieri*), given that Brahmi is a novel material for the synthesis of carbon dots and a medicinal plant. The nanoparticles' size and morphology were analyzed using high-resolution transmission electron microscopy, field emission scanning electron microscopy, and dynamic light scattering techniques, while Raman spectroscopy, Fourier transform infrared spectroscopy), and X-ray diffraction spectroscopy were employed for sample characterization. Optical properties were studied using ultraviolet (UV) and fluorescence spectroscopy. The NCDs showed a high quantum yield of 15.7%, and demonstrated significant fluorescence quenching in the presence of Fe^{3+} and Ni^{2+} ions, with detection limits of 1.46 and 3.19 μmol·L^{-1}, respectively. This rapid, accurate method offers a promising solution for detecting heavy metals in water and could be expanded to real water samples and photocatalytic degradation of methylene blue dye under UV light.

Keywords: *Bacopa monnieri*, metal pollutant, nitrogen doped-carbon dots, bioremediation, biosensing, Ni^{2+}, Fe^{3+}

*** Corresponding author: Saravanan Rajendran,** Instituto de Alta Investigacion, Universidad de Tarapacá, Arica, 1000000, Chile, e-mail: saravanan3.raj@gmail.com
*** Corresponding author: Thanigaivel Sundaram,** Department of Biotechnology, Faculty of Science & Humanities, SRM Institute of Science and Technology, Kattankulathur, Chengalpattu, Tamil Nadu, 603203, India, e-mail: thanigaivel092@gmail.com
*** Corresponding author: Sreeraj Gopi,** Polymers Technology Department, Gdansk University of Technology Building Chemia C, Room 201, Gdansk, Poland, e-mail: drgopisreeraj@gmail.com, tel: +48 58 3472134
*** Corresponding author: Maximilian Lackner,** Department of Industrial Engineering, University of Applied Sciences Technikum Wien, Hoechstaedtplatz 6, 1200, Vienna, Austria, e-mail: maximilian.lackner@technikum-wien.at
Kondetharayil Soman, Sabu Thomas: School of Nanoscience and Nanotechnology, Mahatma Gandhi University, Athirampuzha, 686560, India
Kuppusamy Kanagaraj: Center for Supramolecular Chemistry & Catalysis and Department of Chemistry, College of Science, Shanghai University, Shanghai, 200444, China
Nangan Senthilkumar: Department of Chemistry, Vinayaka Mission's Kirupananda Variyar Arts & Science College, Periyaseeragapdi, Salem, India
Turki Kh. Faraj, Abdulwahed Fahad Alrefaei: Department of Zoology, College of Science, King Saud University, P.O. Box 2455, Riyadh, 11451, Saudi Arabia
Natesan Thirumalaivasan: Department of Periodontics, Saveetha Dental College, and Hospitals, Saveetha Institute of Medical and Technical Sciences (SIMATS), Saveetha University, Chennai, 600077, Tamil Nadu, India
Arpita Roy: Centre for Research Impact and Outcome, Chitkara University, Rajpura, Punjab, 140401, India; Research and Development Cell, Lovely Professional University, Phagwara, 144411, India
Rajan Verma: Chitkara Center for Research and Development, Chitkara University, Baddi, Himachal Pradesh, 174103, India

1 Introduction

According to United Nations sustainable development goals, clean water and sanitation is one of the pivotal elements in people's well-being. Urbanization and new living conditions are creating contamination of main water bodies. People are aware of the gravity of water contamination and how momentous the proper identification and treatment of water have become. The current

access to clean water, for a large number of communities and even countries, is expensive and unreliable, and developing nations cannot bear to use the advanced methodologies for water treatment. A cost-effective biosensor to detect heavy metals in water is therefore desperately needed. This is where the quantum dots (QDs) become important since they can be used as biosensors to find heavy metal ions contained in water. There are several metal-based QDs present such as cadmium, lead, and carbon-based graphene QDs (GQDs). However, they themselves contain toxic substances which constitute a menace to humans and limit the application of QDs. Also, the manufacture technique is quite complex [1,2], leading to expensive sensors. As a result, researchers have considered developing a novel technology; for this reason, carbon dots (CDs) are increasingly being used in biosensor applications. These are ideal nanoparticles because they are made from precursors that are found in nature and have favorable traits like biocompatibility, cytotoxicity, low cost, and ease of production. Also, CDs were found to possess antioxidant and antimicrobial activity. Due to their exquisite properties, CDs enter the biomedical domain fairly quickly which includes drug delivery, bioimaging of microorganisms, cancer cells, and neuro-cells [3], photodynamic therapy, and photothermal therapy [4]. CDs can be used in biosensing applications, due to their high quantum yield (QY) – a measurement of the optical property of CDs that indicates excitation-dependent photoluminescent emission – and stability towards light [5]. Chauhan et al. used a hydrothermal process to produce CDs from coconut coir, obtaining a 48% yield and favorable, low water solubility. They discovered that the excitation wavelength has an effect on the emission spectrum; the highest intensity of emission wavelength was reported to be 530 at 280 nm excitation wavelength. They used pH testing to check the stability of CDs, and the results showed that the CDs were sufficiently stable. Particularly, these CDs can be utilized as effective copper and cadmium metal ion detecting probes [6]. Pacquiao et al. used the same approach to produce CDs from mushrooms, which were then used to detect the presence of Cr^{6+}. Initially, they got a QY of 11%, but surface passivation using tetraethylenepentamine increased the QY to 39% [7]. Chang et al. demonstrated a high QY of 42% CDs utilizing *polygoni multiflori caulis* as a precursor in 2021 [8]. They reported good characteristics, and their CDs were extremely sensitive to Fe^{3+} ions, with a detection limit of 0.025 $\mu mol \cdot L^{-1}$. The hydrothermal process was selected for synthesizing NCDs due to its simplicity, environmental friendliness, and ability to produce uniform, high-quality CDs [9]. This method's long growth period ensures adequate carbonization, leading to high QY, enhanced surface functionality, and improved stability of the CDs [9].

The O–H, N–H, C–H, and COO functionalities that make up the surface of CD can be enhanced by additional doping, which could lead to a higher rate of fluorescence quenching, i.e., the material's fluorescence intensity being reduced [10]. Metal-free CDs are a type of carbon-based nanomaterial known for their biocompatibility, photoluminescence, and low toxicity. In environmental monitoring, they are widely used as sensors for detecting metal ions and pollutants due to their sensitivity and selective interaction with contaminants. In medical applications, CDs serve as bioimaging agents, drug delivery systems, and have potential in cancer diagnostics and therapy owing to their excellent biocompatibility and low toxicity profile. This is the most important aspect of the CDs use in biosensing and the relevant application. Of late, the increase in the number of publications emphasizes the importance of a low-cost biosensor.

In this study, we synthesized nitrogen-doped CDs (NCDs) by using a medicinal plant, Brahmi (*Bacopa Monnieri*), as a precursor. It has been used as ayurvedic medicine for many years, and its therapeutic properties have been reported [10,18]. Because of its antioxidant and anti-inflammation properties, Brahmi is utilized for a variety of purposes. There are bioactive molecules in Brahmi that can function as natural dopants and affect the surface functionalization. Because of its abundance of bioactive surface groups, it may have additional biological activities like antioxidant or antimicrobial capabilities. While past studies on CDs in biosensing emphasize their optical properties and low toxicity, they often overlook long-term stability and specificity in complex environments. Our work addresses these gaps by focusing on metal-free CDs, enhancing stability and selectivity in diverse conditions, thus providing a more sustainable and targeted approach to biosensing applications.

Many heavy metal ion detections employing CDs have long been reported [9,11]; however, Ni^{2+} ion detection is yet to be published. The innovative aspect of this work is the synthesis of CDs from Brahmi, as well as the selective detection of Ni^{2+} ions by this carbon nanomaterial. We conducted morphological, spectroscopic, and optical analyses here. This work helps to understand the effect of doping on QY. We were also interested in how this fluorescence property influences the detection of heavy metal ions; therefore, we conducted a metal sensing investigation. As a result, we obtained an outstanding result for detecting Fe^{3+} and Ni^{2+} ions. Figure 1 illustrates a schematic representation of the synthesis procedure of NCDs and metal ion sensing.

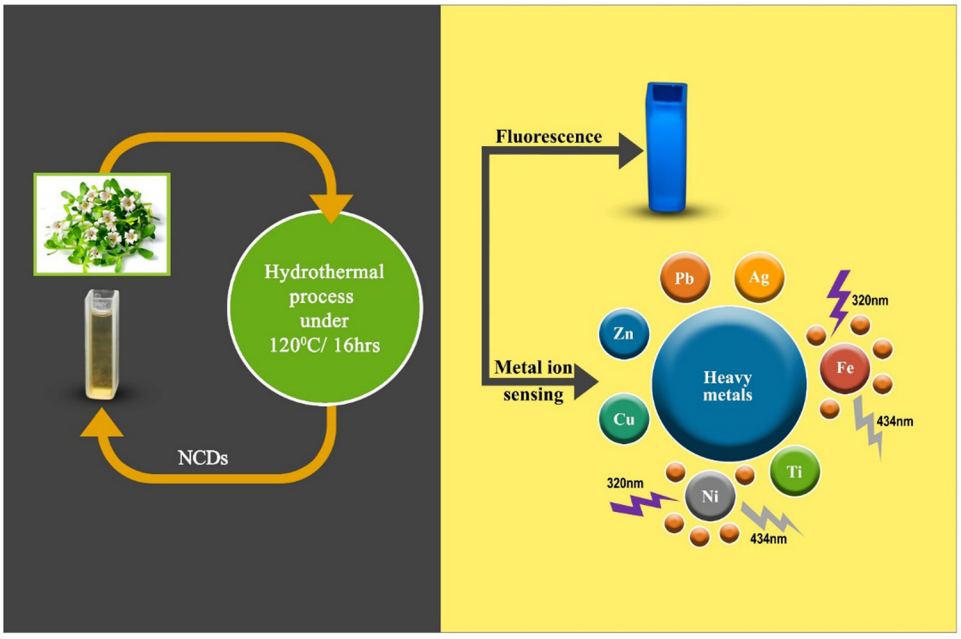

Figure 1: Graphical representation of NCDs synthesis (left) and Ni^{2+} and Fe^{3+} iron probing (right).

2 Materials and methods

2.1 Materials

The medicinal plant Brahmi was collected from a local garden. The chemicals lead(II) acetate (anhydrous), zinc oxide (grade "Hi-LR Himedia"), titanium(IV) dioxide, and dialysis membrane-150, LA401-5MT were purchased from HiMedia (Mumbai, India). Ammonium solution and iron(III) oxide were purchased from Empura. Cupric sulfate pentahydrate and silver nitrate were purchased from Sigma Aldrich. Nickel sulfate and quinine sulfate were purchased from Spectrum and Kemphasol, respectively. All the solutions were made using ultrapure water.

2.2 Synthesis of NCDs from Brahmi

The raw material Brahmi was collected from a local garden, identity-checked, and then thoroughly washed to remove dead leaves and dirt. A grinding machine was used to produce a thick green-colored juice. This juice was then filtered and underwent centrifugation for 20 min at 5,000 rpm and was again passed through the filter. 25 mL of this juice was mixed with 1 mL of ammonium solution, and this mixture was kept in an autoclave for 16 h at 120°C [12]. After that step, the solution was removed from the oven and allowed to cool at room temperature, followed by centrifugation and passing through the filtration process to remove unreacted particles. This solution was finally subjected to a dialysis process, through a dialysis membrane for 3 days. Finally, the authors obtained a dark brown colored liquid containing the NCDs. It was stored below 8°C for further characterization.

2.3 Characterization techniques

The morphological study and particle size distribution were analyzed using Transmission electron microscopy (TEM) from JEOL JEM 2100 (LaB6 Type) at 200 kV. Transmission electron microscopy (TEM) from JEOL JEM 2100 (LaB6 Type) at 200 kV and a field emission scanning electron microscope (FE-SEM) using a MALA3 XMH model (TESCAN BRONO s.r.o., Czech Republic) were used to analyze the morphological study and particle size distribution. The dynamic light scattering (DLS) device HORBIA SZ-100 was used for particle size analysis with a measuring range of 0.3 nm to 8.0 µm. The X-ray diffraction (XRD) patterns were determined using an X-ray spectrometer (Rigaku mini flex bench tops) equipped with a graphite monochromator. For Raman spectroscopic analysis of NCDs, we used an Alpha300RA AFM (WITec GmbH, Ulm, Germany) and RAMAN spectrometer with 532 nm diode-pumped solid-state laser. Fluorescence spectrum analysis has been done using a Perkin Elmer Spectrum Two, and the wavenumber ranges from 400 to 4,000 cm^{-1}. Shimadzu UV-2600 was used to analyze the absorbance spectra of NCDs in the range of 200–800 nm

and fluorescence emission spectra were obtained from a Shimadzu RF-6000 spectro-fluorophotometer.

2.4 Calculation of QY

One of the most important factors to evaluate CDs fluorescent stability and application is their QY, which is simple to ascertain using Eq. 1.

$$QY_S = (F_S A_R QY_S)/(F_R A_S) \quad (1)$$

where QY_S, F_S, and A_S stands for the quantum yield, integrated fluorescence emission, and absorbance of the sample, and QY_R, F_R, and A_R stand for quantum yield, integrated fluorescent emission, and absorbance of the reference. Quinine sulfate (CAS no. 130-95-0) is used as the reference material, and its QY is 54% in a 0.1 N solution of H_2SO_4 [13].

2.5 Metal ion detection

For the metal ion detection analysis, 500 µM metal ion solutions were prepared for each metal salt. Then, 1 mL of synthesized NCDs was added to the metal ion solution, and after a few minutes, the solution was subjected to fluorescent microscopic analysis to check the fluorescent quenching of NCDs by comparing with the intensities of pure NCDs and a solution with NCDs and metal ions [10]. To analyze the concentration dependence on fluorescent quenching, the concentration of metal ions was varied from 50 to 500 µM.

3 Results and discussion

Prepared CDs were characterized by various techniques and was used based on their utility. Generally, TEM analysis provides crucial insights into the morphological structure and particle size distribution of CDs, directly aligning with the research objective of understanding nanoparticle formation. FTIR helps identify surface functional groups, offering important information on the chemical composition and bonding of the CDs. Spectroscopic analysis, such as ultraviolet-visible (UV-Vis) and XPS, reveals electron-level distribution and surface states, essential for characterizing optical properties. Fluorescence spectroscopy is the primary technique for evaluating the photoluminescence behavior of the CDs, which is key to their application in sensing and bioimaging.

Initially, the morphology and the particle size of synthesized NCDs are calculated using high resolution-transmission electron microscopy (HR-TEM) and is shown in Figure 2a and b. The NCDs are spherical in shape, with an average particle size distribution range of 2.54–3.27 nm and a d-spacing of 0.24 nm (the minimum distance between two parallel planes of atoms), as determined by this analysis. These findings can be compared to the study by Atchudan et al., who reported on NCDs [14]. They obtained NCDs with a particle size of the same range as that of our studies, and QY is relatively high in this study, at 15.76%.

The FE-SEM analysis of this study gives an excellent illustration of NCDs morphology. Figure 2c depicts the FE-SEM image, which demonstrates the spherical shape of the produced NCDs and gives support to the TEM report. The DLS analysis is shown in Figure 2d. The mean diameter of the nanoparticle was found to be 2.54 nm with a monodisperse distribution.

Figure 3a shows the FTIR spectra of NCDs, which are used to identify the surface functional groups of NCDs, with distinctive absorption bands appearing at 3,261 cm^{-1} for O–H and N–H stretching vibrations, while 2,176 and 1,080 cm^{-1} represent the C═N and C–O bonds, respectively, and 1,634 cm^{-1} for C═C or NH_2 stretching vibrations. Furthermore, a considerable number of aromatic alkoxy groups are allocated to bands in the 1,050–1,360 cm^{-1} range [15].

All of the foregoing findings show that hydroxyl and carboxylic groups are present on the surface of NCDs, which enhances the optical and surface properties of NCDs. Figure 3b shows the XRD pattern of the NCDs. The broad peak verifies the amorphous nature of CDs and is detected at $2\theta = 23°$. Using the Bragg equation, the d spacing obtained was 0.39, which is close to the d spacing value obtained from HR-TEM analysis. The amorphous character of NCDs is caused by an increase in the d spacing value. These results are consistent with NCDs made from *Chionanthus retusus* fruit extract [14,16].

$$n\lambda = 2d \sin\theta \quad (2)$$

where the value of n is 1, the incident X-ray wavelength is λ = 1.54 Å, and the angle between the incident rays and the surface of the materials is θ. Figure 4a shows the emission peak at 434 nm, which corresponds to a 320 nm excitation wavelength. Under ambient light, the diluted NCDs aqueous solution appears pale yellow, but when exposed to UV–light (λ = 365 nm), it turns to a highly strong blue color. Excitation-dependent emission spectra of NCDs are shown in Figure 4b, and the excitation wavelengths ranged from 320 to 550 nm in this experiment [17]. The surface functionalities of NCDs have a

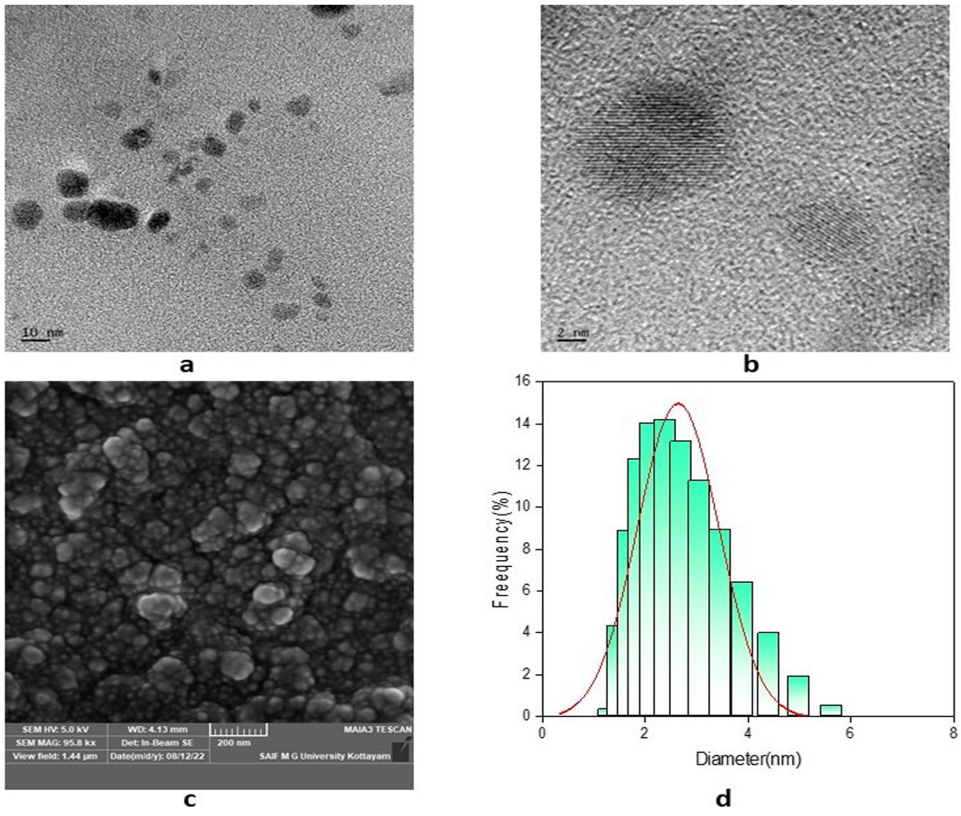

Figure 2: (a) and (b) HR-TEM image of NCDs, (c) FE-SEM of NCDs, and (d) DLS analysis.

considerable number of electronic states, which causes this excitation-dependent emission characteristics [18]. The graph shows that by varying the excitation wavelength, the peak centers were red shifted (Figure 4b). These findings can be compared to the NCDs studies by Zulfajri et al., where highest fluorescence intensity was obtained at 350 nm excitation wavelength, and the maximum intensity was reported here at 360 nm [19].There is no significant emission peak after 550 nm [20].

The UV-vis absorption spectrum of the NCDs in Figure 4c shows two strong absorption bands, which are typical of an aromatic system's absorption. The n–π* transition with C═N bonds is responsible for the first absorption band, which was found at 214 nm [21]. At 267 nm, the π–π*

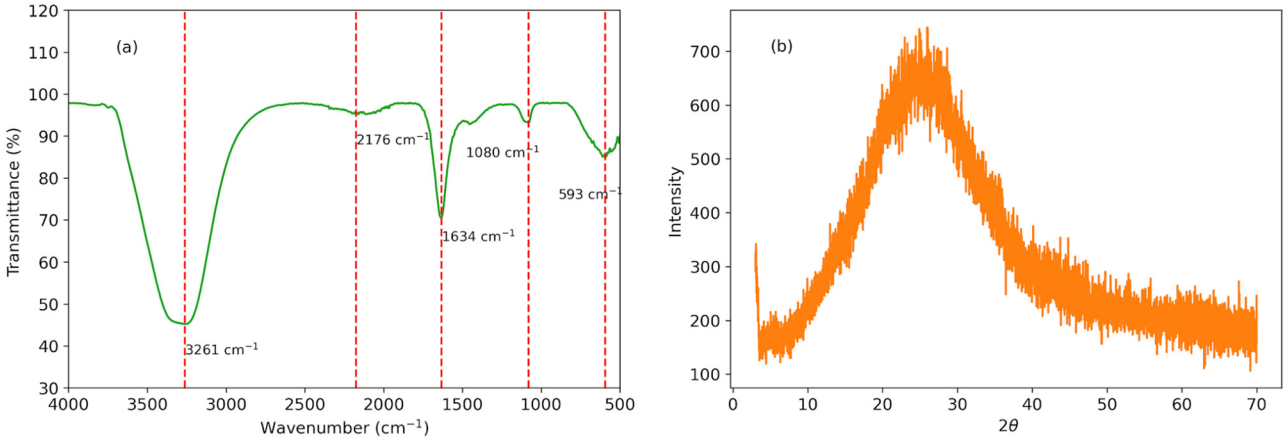

Figure 3: (a) FTIR spectrum and (b) XRD pattern of NCDs.

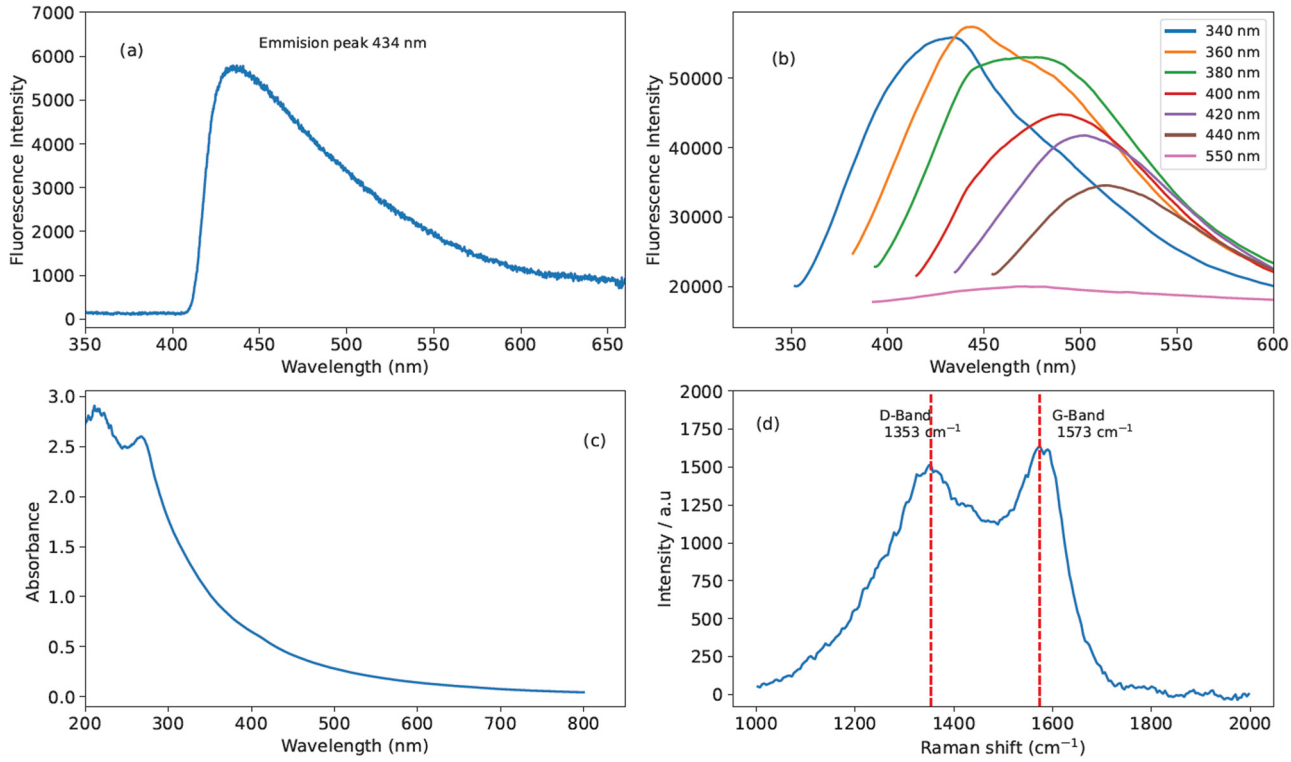

Figure 4: (a) Fluorescence microscopy of NCDs, (b) Excitation-dependent PL intensity of NCDs, (c) UV spectroscopy, and (d) Raman spectroscopy.

transition with C═C bonds for aromatic sp^2 hybridization was detected, which is related to the second characteristic absorption peak. These NCDs appear pale yellow in natural light and blue under 365 nm UV irradiation. Raman spectroscopy provides vital information on the structural defects, degree of graphitization, and vibrational modes of CDs, aiding in the understanding of their molecular structure and carbon backbone, which is crucial for tuning their optical and electronic properties. Figure 4d illustrates the Raman spectrum of NCDs, which indicates a D-band at 1,353 cm^{-1}, demonstrating the presence of sp^2 hybridized carbon systems, and a G-band at 1,573 cm^{-1} represents the sp^3 hybridization [22]. The ID/IG (D band to G band intensity ratio) values were used to determine the graphitization of carbon nanostructured materials. Because of the strong fluorescence background, the ID/IG value is 0.86, and the intensity ratio of the D to the G-band suggests that the synthesized NCDs had a mild graphitic character. This ID/IG ratio is also a measure of defects in the carbon nanomaterials. These results closely correspond to the findings of authors who have systematically studied the ID/IG ratio [23].

4 Metal ion detection

The test was carried out using various metal ions: Ag^{+}, Zn^{2+}, Ti^{4+}, Pb^{2+}, Ni^{2+}, Fe^{3+}, and Cu^{2+} in the presence of NCDs at a concentration of 500 µM. Figure 5a shows the fluorescence quenching of NCDs in the presence of these metal ions. Each of these metal ion shows different photoluminescence (PL) intensities, but in Figure 5a nickel and iron PL graphs show a deep quenching of NCDs fluorescence [24,25].

The quenching rate of NCDs is depicted in the diagram in Figure 5b. Functionalities seen on the surface of NCDs are too responsible for this quenching mechanism. The metal ion contained in the NCDs was shown to have a strong affinity by these surface functions. Figure 6a shows how the concentration of Fe^{3+} ions affect the quenching rate here varied the concentration of metal ion from 50 to 500 µM. From this graph it is very clear that increasing the concentration of metal ion decreased the fluorescent intensity. Figure 6b also shows the same analysis of Ni^{2+} ions [26]. From these two graphical representations, 500 µM shows the high fluorescent intensity of quenching. Upon addition of metal ions to CDs, the fluorescence quenching in CDs may

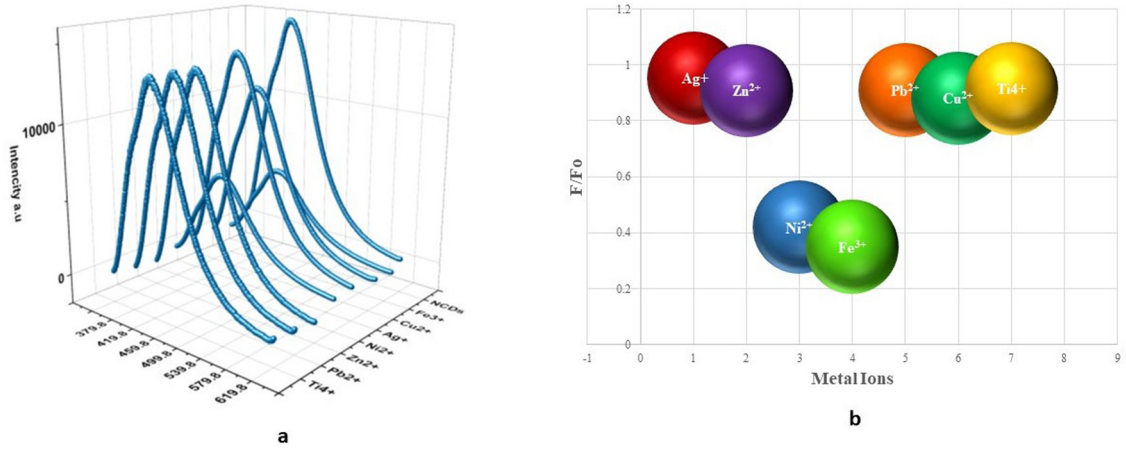

Figure 5: (a) Fluorescence quenching analysis of metal ions Ag^{+}, Zn^{2+}, Ti^{4+}, Pb^{2+}, Ni^{2+}, Fe^{3+}, and Cu^{2+} at a concentration of 500 µm and (b) quenching comparison of Ag^{+}, Zn^{2+}, Ti^{4+}, Pb^{2+}, Ni^{2+}, Fe^{3+}, and Cu^{2+}.

occur due to multiple factors like photoinduced electron transfer, energy transfer, charge transfer, and aggregation, leading to the complete decay of their luminescence.

The interaction between fluorescence intensity and metal ion concentrations is shown linearly in Figure 6c and d. The obtained R^2 value of 0.9722 for Fe^{3+} ions and 0.971 for Ni^{2+} ions indicated good linearity in the outcome. It is determined that the Fe^{3+} ion's limit of detection (LOD) is 1.46 and the LOD of Ni^{2+} ions is 3.19.

Table 1 compares the LOD (limit of detection) value of CDs synthesized from various raw materials. NCDs generated in this study had an excellent LOD value for Fe^{3+} ion detection when compared to CDs prepared from blueberry [29] and L-glutamic acid [31]. The value of the other reports in the table is comparable to that of our findings. Ni^{2+} detection studies are few in the literature; however, CDs synthesized from imidazole [26] reported Ni^{2+} detection with a LOD of 0.93 mM, which is greater than our findings.

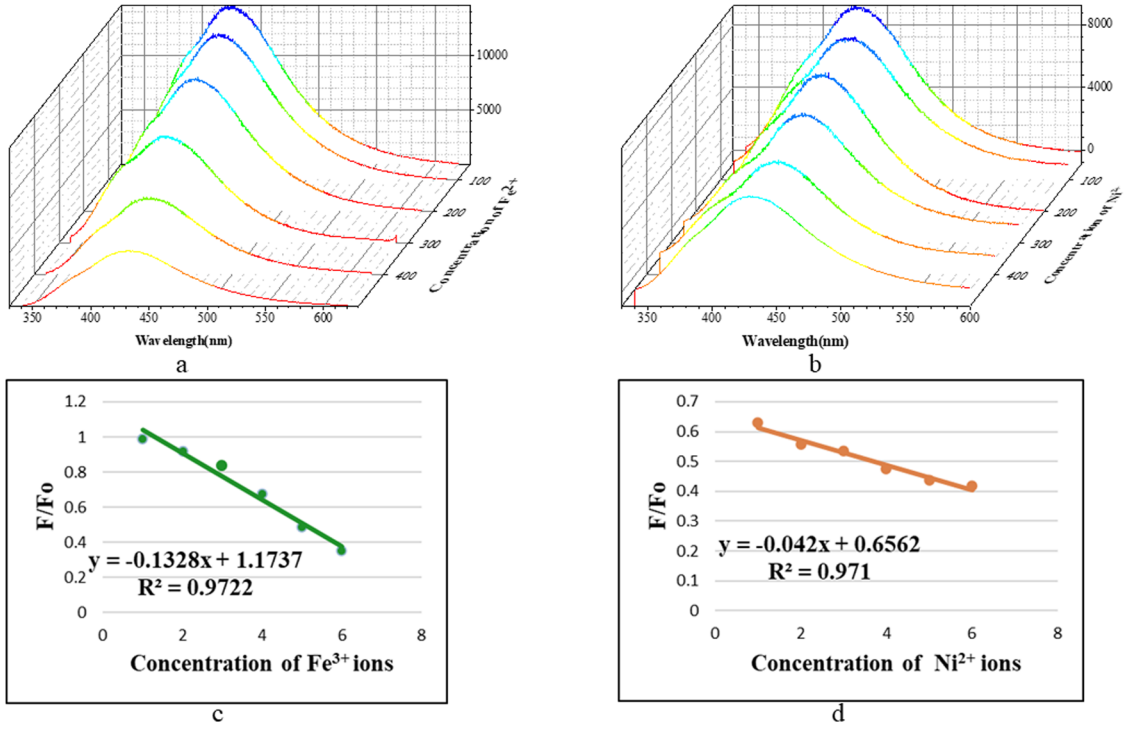

Figure 6: Quenching rate analysis at varying concentrations (a) Fe^{3+} ions and (b) Ni^{2+} ions. The fluorescent intensity ratios of NCDs versus the concentrations of (c) Fe^{3+} ions and (d) Mn^{2+} ions.

Table 1: Comparison of limit of detection values of biosensors made from CDs

Sl. no.	Carbon precursor	Metal ions	Linear range	LOD (μM)	Ref.
1	Wheat straw	Fe^{3+}	0–250 μM	1.95	[27]
2	Oxidized cellulose	Fe^{3+}	0–100 μM	1.14	[28]
3	Blueberry	Fe^{3+}	12.5–100 μM	9.97	[29]
4	Food waste	Fe^{3+}	12.5–100 μM	32	[30]
5	CDs from L-glutamic acid	Fe^{3+}	0–50 μM	4.64	[31]
6	CDs from graphite	Fe^{3+}	1–100 μM	1	[32]
8	Cellulose fibers	Fe^{3+}	25–250 μM	0.96	[33]
9	CD-imidazole	Ni^{2+}	6–100 (mM)	0.93 (mM)	[26]
10	*Poa pratensis*	Fe^{3+}	5–25 μM	1.4	[34]
11	*Bacopa monnieri* (this work)	Fe^{3+}	5–500 μM	1.46	This work
	Bacopa monnieri (this work)	Ni^{2+}	5–500 μM	3.19	This work

The performance of a biosensor is good with lower LOD values and these findings demonstrated that, this sensing probe is an excellent tool for detecting Ni^{2+} and Fe^{3+} ions.

4.1 Real sample analysis: Determination of Fe^{3+} and Ni^{2+} ion levels in real water samples

For the purpose of exploring the possible benefits and realistic application of the generated NCDs to actual/real samples (which were collected from various water sources), the levels of Fe^{3+} and Ni^{2+} ions were measured in seven real-world water samples: drinking water, tap water, well water, bore well water, river water, sea water, and two waste water samples. Before being used, all obtained water samples were filtered three times with qualitative filter paper, and the initial concentrations of Fe^{3+} and Ni^{2+} ions were measured. Fe^{3+} and Ni^{2+} ions were added in increments of 20, 40, and 60 mm to the aforementioned water samples using the usual addition method to measure the concentration of these two ions. The data obtained demonstrate that NCDs enable good recovery in the measurement of spiking Fe^{3+} and Ni^{2+} ion concentrations (Table 2).

4.2 Photocatalytic activity of MB under UV light

In photocatalysis, a chemical reaction is accelerated by visible, infrared, or UV light while a photocatalyst is present to absorb light and change reaction partners. For instance, light can be harvested by CDs via chemical transformation, excitation, and direct absorption. Methylthioninium chloride, commonly called methylene blue (CA No. 61-73-4), is a salt used as a dye and as a medication, with the formula $C_{16}H_{18}ClN_3S$. The photocatalytic degradation of methylene blue in the presence of NCDs has been used to evaluate under UV light (Figure 7).

Upon increasing the time, the methylene blue absorption peaks are decreased, which indicates the dye is degraded in the presence of NCDs. It is an interesting application, which uses the prepared NCDs to treat the polluted dye water.

5 Conclusion

Water contamination has caused a decrease in aquatic biodiversity and a rise in hazardous drinking water. Clean water is critical for ecological balance and public health. Biosensing with the novel NCDs reported here is an efficient method for detecting the presence of Fe^{3+} and Ni^{2+} ions in bodies of water. The obtained LOD value for Fe^{3+} ion is 1.46 μM, which is lower than the permissible level advised by the US Environmental Protection Agency, and the LOD value of Ni^{2+} is 3.19 μM, which is lower than previously reported. Further, we extend the potential utility of the produced NCDs for the detection of metal ions in various water sources as real sample analysis and sensor for photocatalytic dye degradation of methylene blue dye. This work demonstrates the potential for low-cost, heavy-metal free sensors for Fe^{3+} and Ni^{2+} in water, and its efficacy in different water samples could be demonstrated. In future CDs have the potential to combine with other semiconductors for high-efficiency hydrogen production. They can improve the efficiency of solar-to-hydrogen conversion

Table 2: Analytical results for the detection of Fe^{3+} and Ni^{2+} ions in five practical samples

Sample	Metal ion determined (μM)[a]	Metal ion added (μM)	Metal ion expected (μM)	Metal ion found (μM)[a]	Recovery (%)
For Ni^{2+} ions					
Drinking water	0.39 ± 0.3	10	10.39	10.42 ± 0.3	100.3
		20	20.39	20.35 ± 0.2	99.8
		30	30.39	30.31 ± 0.4	99.7
Tap water	1.13 ± 0.5	10	11.13	11.18 ± 0.5	100.5
		20	21.13	20.37 ± 0.3	96.4
		30	31.13	31.07 ± 0.8	99.8
Well water	2.21 ± 0.2	10	12.21	12.12 ± 0.5	99.3
		20	22.21	22.22 ± 0.4	100
		30	32.21	31.16 ± 0.7	96.7
Bore well water	2.43 ± 0.3	10	12.43	12.11 ± 0.5	97.4
		20	22.43	22.47 ± 0.3	100.2
		30	32.43	32.12 ± 0.6	99
River water #1	2.76 ± 0.2	10	12.76	12.68 ± 0.8	99.4
		20	22.76	22.74 ± 0.9	99.9
		30	32.76	32.79 ± 0.5	100
Sea water	3.12 ± 0.7	10	13.12	13.08 ± 0.4	99.7
		20	23.12	23.14 ± 0.3	100.1
		30	33.12	33.04 ± 0.7	99.8
Waste water #1	7.97 ± 0.9	10	17.97	17.99 ± 0.4	100.1
		20	27.97	27.91 ± 0.7	99.8
		30	37.97	37.99 ± 0.2	100.1
Waste water #2	8.44 ± 0.9	10	18.44	18.45 ± 0.4	100.1
		20	28.44	28.40 ± 0.5	99.9
		30	38.44	38.45 ± 0.3	100
For Fe^{3+} ions					
Drinking water	5.47 ± 0.4	10	15.47	15.48 ± 0.4	100
		30	35.47	35.44 ± 0.5	99.9
		50	55.47	55.49 ± 0.2	100
Tap water	6.62 ± 0.5	10	16.62	16.63 ± 0.5	100
		30	36.62	36.68 ± 0.3	100.2
		50	56.62	56.58 ± 0.2	99.9
Well water	8.33 ± 0.9	10	18.33	18.0 ± 0.5	98.2
		30	38.33	38.35 ± 0.3	100.1
		50	58.33	58.12 ± 0.2	99.6
Bore well water	9.72 ± 0.3	10	19.72	19.12 ± 0.5	97.0
		30	39.72	39.74 ± 0.3	100.1
		50	59.72	59.67 ± 0.4	99.9
River water #1	10.13 ± 0.4	10	20.13	20.19 ± 0.6	100.3
		30	40.13	39.11 ± 0.7	97.5
		50	60.13	60.09 ± 0.8	99.9
Sea water	10.91 ± 0.7	10	20.91	20.95 ± 0.4	100.2
		30	40.91	40.89 ± 0.3	100
		50	60.91	60.10 ± 0.5	98.7
Waste water #1	12.72 ± 0.9	10	22.72	22.82 ± 0.4	100.4
		30	42.72	42.54 ± 0.7	99.6
		50	62.72	62.76 ± 0.3	100.1
Waste water #2	13.22 ± 0.4	10	23.22	20.23 ± 0.8	87.1
		30	43.22	43.27 ± 0.4	100.1
		50	63.22	63.24 ± 0.3	100

[a]Mean value ± standard deviation (n = 3).

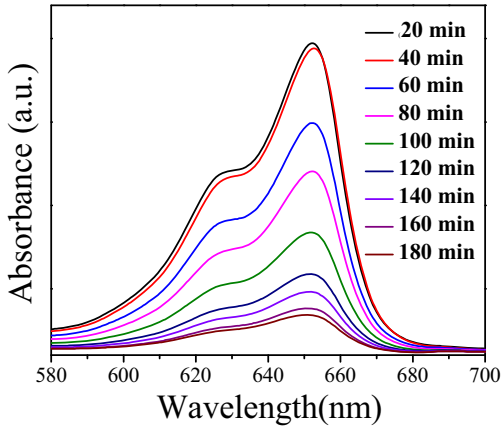

Figure 7: Photocatalytic degradation of methylene blue. UV absorption spectra of methylene blue and prepared NCDs in the UV light at different time intervals (20–180 min).

in photocatalytic water splitting. In waste water, organic pollutants such as dyes and medications can be greatly broken down by CDs. This has the potential to improve the industrial waste water treatment and air purification systems. Moreover, they are capable of cleaning up dangerous substances like poisonous heavy metals and oil spills.

Acknowledgments: We extend our appreciation to the Researchers Supporting Project at King Saud University, Riyadh, Saudi Arabia, for funding this research project, (Fund no. RSP2025R218).

Funding information: This research was funded by Researchers Supporting Project at King Saud University, Riyadh, Saudi Arabia, Fund no. RSP2025R218.

Author contributions: Kondetharayil Soman and Nangan Senthilkumar: writing – original draft, resources, investigation, data curation, and conceptualization. Kuppusamy Kanagaraj and Natesan Thirumalaivasan: writing – original draft, resources, and formal analysis. Turki Kh. Faraj and Abdulwahed Fahad Alrefaei: project administration and investigation. Arpita Roy and Rajan Verma: formal analysis, data curation, and conceptualization. Sabu Thomas, Saravanan Rajendran, Thanigaivel Sundaram, Sreeraj Gopi, and Maximilian Lackner: writing – review and editing, visualization, validation, supervision, resources, and conceptualization.

Conflict of interest: Authors state no conflict of interest.

Data availability statement: The datasets generated during and/or analyzed during the current study are available from the corresponding author on reasonable request.

References

[1] Hu L, Zhang C, Zeng G, Chen G, Wan J, Guo Z, et al. Metal-based quantum dots: synthesis, surface modification, transport and fate in aquatic environments and toxicity to microorganisms. RSC Adv. 2016;6:78595–610.

[2] Qiu J, Li D, Mou X, Li J, Guo W, Wang S, et al. Effects of graphene quantum dots on the self-renewal and differentiation of mesenchymal stem cells. Adv Healthc Mater. 2016;5:702–10.

[3] Zheng M, Ruan S, Liu S, Sun T, Qu D, Zhao H, et al. Self-targeting fluorescent carbon dots for diagnosis of brain cancer cells. ACS Nano. 2015;9:11455–61.

[4] Bao X, Yuan Y, Chen J, Zhang B, Li D, Zhou D, et al. In vivo theranostics with near-infrared-emitting carbon dots—highly efficient photothermal therapy based on passive targeting after intravenous administration. Light: Sci Appl. 2018;7:91.

[5] Hong WT, Yang HK. Luminescent properties of carbon dots originated from pine pollen for anti-counterfeiting application. Opt Laser Technol. 2022;145:107452.

[6] Chauhan P, Dogra S, Chaudhary S, Kumar R. Usage of coconut coir for sustainable production of high-valued carbon dots with discriminatory sensing aptitude toward metal ions. Mater Today Chem. 2020;16:100247.

[7] Pacquiao MR, de Luna MDG, Thongsai N, Kladsomboon S, Paoprasert P. Highly fluorescent carbon dots from enokitake mushroom as multi-faceted optical nanomaterials for Cr6+ and VOC detection and imaging applications. Appl Surf Sci. 2018;453:192–203.

[8] Chang D, Zhao Z, Niu W, Shi L, Yang Y. Iron ion sensing and in vitro and in vivo imaging based on bright blue-fluorescent carbon dots. Spectrochim Acta Part A: Mol Biomol Spectrosc. 2021;260:119964.

[9] Atchudan R, Edison TNJI, Perumal S, Muthuchamy N, Lee YR. Hydrophilic nitrogen-doped carbon dots from biowaste using dwarf banana peel for environmental and biological applications. Fuel. 2020;275:117821.

[10] Wei LF, Chen CY, Lai CK, Thirumalaivasan N, Wu SP. A nano-molar fluorescent turn-on probe for copper (II) detection in living cells. Methods. 2019;168:18–23.

[11] Singh J, Kaur S, Lee J, Mehta A, Kumar S, Kim K-H, et al. Highly fluorescent carbon dots derived from Mangifera indica leaves for selective detection of metal ions. Sci Total Environ. 2020;720:137604.

[12] Sachdev A, Gopinath P. Green synthesis of multifunctional carbon dots from coriander leaves and their potential application as antioxidants, sensors and bioimaging agents. Analyst. 2015;140:4260–9.

[13] Yu J, Song N, Zhang Y-K, Zhong S-X, Wang A-J, Chen J. Green preparation of carbon dots by Jinhua bergamot for sensitive and selective fluorescent detection of Hg^{2+} and Fe^{3+}. Sens Actuators B: Chem. 2015;214:29–35.

[14] Atchudan R, Kishore SC, Gangadaran P, Edison TNJI, Perumal S, Rajendran RL, et al. Tunable fluorescent carbon dots from biowaste as fluorescence ink and imaging human normal and cancer cells. Environ Res. 2022;204:112365.
[15] Atchudan R, Edison TNJI, Mani S, Perumal S, Vinodh R, Thirunavukkarasu S, et al. Facile synthesis of a novel nitrogen-doped carbon dot adorned zinc oxide composite for photodegradation of methylene blue. Dalton Trans. 2020;49:17725–36.
[16] Jin H, Gui R, Wang Y, Sun J. Carrot-derived carbon dots modified with polyethyleneimine and nile blue for ratiometric two-photon fluorescence turn-on sensing of sulfide anion in biological fluids. Talanta. 2017;169:141–8.
[17] Ramezani Z, Qorbanpour M, Rahbar N. Green synthesis of carbon quantum dots using quince fruit (Cydonia oblonga) powder as carbon precursor: application in cell imaging and As^{3+} determination. Colloids Surf A: Physicochem Eng Asp. 2018;549:58–66.
[18] Shahraki HS, Bushra R, Shakeel N, Ahmad A, Ahmad M, Ritzoulis C. Papaya peel waste carbon dots/reduced graphene oxide nanocomposite: from photocatalytic decomposition of methylene blue to antimicrobial activity. J Bioresour Bioprod. 2023;8:162–75.
[19] Zulfajri M, Sudewi S, Damayanti R, Huang GG. Rambutan seed waste-derived nitrogen-doped carbon dots with l-aspartic acid for the sensing of Congo red dye. RSC Adv. 2023;13:6422–32.
[20] Shen J, Shang S, Chen X, Wang D, Cai Y. Facile synthesis of fluorescence carbon dots from sweet potato for Fe^{3+} sensing and cell imaging. Mater Sci Eng: C. 2017;76:856–64.
[21] Huang H, Lv J-J, Zhou D-L, Bao N, Xu Y, Wang A-J, et al. One-pot green synthesis of nitrogen-doped carbon nanoparticles as fluorescent probes for mercury ions. RSC Adv. 2013;3:21691–6.
[22] Zhou J, Sheng Z, Han H, Zou M, Li C. Facile synthesis of fluorescent carbon dots using watermelon peel as a carbon source. Mater Lett. 2012;66:222–4.
[23] Arul V, Sethuraman MG. Hydrothermally green synthesized nitrogen-doped carbon dots from Phyllanthus emblica and their catalytic ability in the detoxification of textile effluents. ACS Omega. 2019;4:3449–57.
[24] Dineshkumar R, Murugan N, Rani JA, Arthanareeswari M, Kamaraj P, Devikala S, et al. Synthesis of highly fluorescent carbon dots from Plectranthus amboinicus as a fluorescent sensor for Ag^{+} ion. Mater Res Express. 2019;6:104006.
[25] Thirumalaivasan N, Venkatesan P, Wu SP. Highly selective turn-on probe for H2S with imaging applications in vitro and in vivo. N J Chem. 2017;41(22):13510–5.
[26] Gong Y, Liang H. Nickel ion detection by imidazole modified carbon dots. Spectrochim Acta Part A: Mol Biomol Spectrosc. 2019;211:342–7.
[27] Yuan M, Zhong R, Gao H, Li W, Yun X, Liu J, et al. One-step, green, and economic synthesis of water-soluble photoluminescent carbon dots by hydrothermal treatment of wheat straw, and their bio-applications in labeling, imaging, and sensing. Appl Surf Sci. 2015;355:1136–44.
[28] Liu Z, Chen M, Guo Y, Zhou J, Shi Q, Sun R. Oxidized nanocellulose facilitates preparing photoluminescent nitrogen-doped fluorescent carbon dots for Fe^{3+} ions detection and bioimaging. Chem Eng J. 2020;384:123260.
[29] Aslandaş AM, Balcı N, Arık M, Şakiroğlu H, Onganer Y, Meral K. Liquid nitrogen-assisted synthesis of fluorescent carbon dots from Blueberry and their performance in Fe^{3+} detection. Appl Surf Sci. 2015;356:747–52.
[30] Podder A, Thirumalaivasan N, Chao YK, Kukutla P, Wu SP, Bhuniya S. Two-photon active fluorescent indicator for detecting NADH dynamics in live cells and tumor tissue. Sens Actuators B: Chem. 2020;324:128637.
[31] Yu J, Xu C, Tian Z, Lin Y, Shi Z. Facilely synthesized N-doped carbon quantum dots with high fluorescent yield for sensing Fe^{3+}. N J Chem. 2016;40:2083–8.
[32] Nguyen V, Yan L, Si J, Hou X. Femtosecond laser-assisted synthesis of highly photoluminescent carbon nanodots for Fe^{3+} detection with high sensitivity and selectivity. Opt Mater Express. 2016;6:312–20.
[33] Yang G, Wan X, Su Y, Zeng X, Tang J. Acidophilic S-doped carbon quantum dots derived from cellulose fibers and their fluorescence sensing performance for metal ions in an extremely strong acid environment. J Mater Chem A. 2016;4:12841–9.
[34] Krishnaiah P, Atchudan R, Perumal S, Salama E-S, Lee YR, Jeon B-H. Utilization of waste biomass of Poa pratensis for green synthesis of N-doped carbon dots and its application in detection of Mn^{2+} and Fe^{3+}. Chemosphere. 2022;286:131764.